A&A 402, 1021–1032 (2003)
DOI: 10.1051/0004-6361:20030165
© ESO 2003

Astronomy & Astrophysics

BeppoSAX observations of two unclassified LMXBs: X1543–624 and X1556–605

R. Farinelli[1], F. Frontera[1,2], N. Masetti[2], L. Amati[2], C. Guidorzi[1], M. Orlandini[2], E. Palazzi[2], A. N. Parmar[3], L. Stella[4], M. Van der Klis[5], and S. N. Zhang[6]

[1] Dipartimento di Fisica, Universitá di Ferrara, via Paradiso 12, 44100 Ferrara, Italy
[2] Istituto Astrofisica Spaziale e Fisica Cosmica, Sezione di Bologna, CNR, Via Gobetti 101, 40129 Bologna, Italy
[3] Astrophysics Division, Space Science Department of ESA, ESTEC, PO Box 299, 2200 AG Noordwijk, The Netherlands
[4] Osservatorio Astronomico di Roma, Via Frascati, 33, 00040 Monteporzio Catone, Italy
[5] Astronomical Institute "Anton Pannekoek", University of Amsterdam and Center of High Energy Astrophysics, Kruislaan 403, 1098 SJ Amsterdam, The Netherlands
[6] Department of Physics, University of Alabama in Huntsville, Huntsville, AL 35899, USA

Received 6 May 2002 / Accepted 8 January 2003

Abstract. Observations of two unclassified Low Mass X–ray Binaries, X1543–624 and X1556–605, are presented. In the 2–10 keV band the first of the two sources is a factor of two stronger than the other. Both sources do not show X–ray bursts, dips or eclipses in their X–ray light curves. We find that both spectra are described by a two–component model consisting of emission from a cool accretion disk plus a Comptonized blackbody with $kT_{\rm bb} \sim 1.5$ keV in a low opacity plasma. The spectrum of X1543–624 hardens from the first to the second observation, when the source slowly moves from right to left in the colour–colour diagram. The spectrum of X1556–605 can also be described by a model consisting of a blackbody plus an unsaturated Comptonization with electron energy $kT_{\rm e} \sim 4$ keV. In the first observation, X1543–624 shows evidence of a Fe K emission line at 6.4 keV. Moreover, in both observations, the source spectrum exhibits an emission feature around 0.7 keV, which is interpreted as due to the superposition of the K edge absorption features of O and Ne elements with uncommon relative abundances with respect to the solar one ($\rm O/O_{\odot} \sim 0.3$, $\rm Ne/Ne_{\odot} \sim 2.5$). In the spectrum of X1556–605 no emission lines are observed. We discuss these results and their implications for the source classification and the accretion geometry of the compact object.

Key words. stars: individual: X1543–624; X1556–605 – X–rays: general – X–rays: stars – stars: neutron – accretion, accretion disks

1. Introduction

Low Mass X–ray Binaries (LMXBs) form the most populated class of galactic X–ray binaries. These objects are formed by late–type secondary stars, with mass typically less than 1 $M_{\odot}$, which transfers matter onto a highly compact primary via Roche lobe overflow. These systems mostly contain old, low magnetic field ($<10^9$ G) neutron stars (NS) as compact primaries, and are characterized by persistent, albeit variable, X–ray emission. The accreting matter carries large angular momentum and this implies the formation of an accretion disk around the compact object; then, X–ray emission mainly arises from the inner parts of the disk and around the accreting primary, in the so–called boundary layer. This mechanism ensures quite high efficiency in the conversion of gravitational energy into X–rays, and luminosities above 10^{36} erg s^{-1} are quite common among LMXBs.

The most successful classification of LMXBs comes from their X–ray "colour" behaviour (Hasinger & van der Klis 1989). On the basis of this classification, LMXBs are subdivided into Z sources and atoll sources, from the shape of their track in the X–ray colour–colour diagram (CD) and on the different timing behaviour that correlates with the position on the tracks. The observed time scales taken to track their CD are shorter (hours or days) for Z sources than for atoll sources (weeks or months). LMXBs belonging to the atoll sources usually have luminosities lower than Z sources, typically in the range 0.01–$0.1\times L_{\rm Edd}$. They are observed in either soft ("banana") or hard ("island") state: in the latter case they show, above 10 keV, power–law ( ) spectral shapes with typical high–energy cut–offs $E_{\rm c} \lesssim 100$ keV, except a few peculiar cases, like Aql X–1 (Harmon et al. 1996) and 4U 0614+09 (Piraino et al. 1999); the contribution of the high energy component with respect to the total flux can be very high (e.g., about 50% of the total flux in the case of 4U1705-44, Barret et al. 1996). It has been demonstrated (e.g., van der Klis et al. 1990; van der Klis 1995) that the source state along the CD track correlates well with the mass accretion rate $\dot{M}$, and the hard state (island) occurs preferrably at low $\dot{M}$.

Send offprint requests to: F. Frontera, e-mail: fontera@fe.infn.it

Table 1. Log of the four *BeppoSAX* NFI observations presented in this work.

Source	Obs.	Start time (UT)	End time (UT)	LECS ksec	MECS ksec	HPGSPC ksec	PDS ksec	2–10 keV MECS count rate (s^{-1})
X1543–624	1	1997 Feb 21 09:38:02	1997 Feb 21 17:39:50	6.6	16.6	7.5	7.5	12.8
	2	1997 Apr 1 22:38:29	1997 Apr 2 05:54:05	6.6	18.3	7.8	8.1	11.4
X1556–605	1	1997 Mar 10 17:10:02	1997 Mar 10 23:58:50	7.3	17.9	7.9	7.9	5.42
	2	1997 Apr 3 18:08:47	1997 Apr 4 01:54:50	5.1	17.8	7.3	7.7	5.69

Spectra of Z sources are generally much softer. In the eighties they were usually described in terms of a blackbody ( ) plus an additional component: either an unsaturated Comptonization spectrum (the "Western model", White et al. 1986, 1988), approximated by the function $I(E) \propto E^{-\Gamma} \exp[-E/kT_{\rm e}]$ ( ) or the solution of the Kompaneets equation given by Sunyaev & Titarchuk (1980), or a multi–colour disk blackbody (, the "Eastern model", Mitsuda et al. 1984). Later Mitsuda et al. (1989) refined the Eastern model by replacing the with a Comptonized and successfully applied it to the atoll source X1608–522. In the 1–10/20 keV energy range, the classical Western and Eastern models have also been used to describe spectra of atoll sources (e.g., White et al. 1988, Asai et al. 2000, hereafter A2000). Also other models, like or , plus the Comptonization model worked out by Titarchuk (1994) have been adopted to describe spectra of Z sources (e.g., Di Salvo et al. 2001, 2002). Recently it has been found that most of the classical Z sources (GX 5–1, Asai et al 1994; Cyg X–2, Frontera et al. 1998, Di Salvo et al. 2002; GX 17+2, Di Salvo et al. 2000a; GX 349+2, Di Salvo et al. 2001; Sco X–1, D'Amico et al. 2001), and Cir X-1 (Iaria et al. 2001) show in their spectra a hard X–ray tail. The tail is observed only during some positions of the sources along their CD, with no general rule: e.g., in GX17+2 the hard tail is apparent during the Horizontal Branch, in GX349+2 it is detected during the Flaring Branch, in Sco X–1 it is detected in all the three branches of the Z pattern.

It is still not clear what determines the presence of the high energy component in Z sources and whether this component evolves with continuity from atoll sources to Z sources. Recently Gierliński & Done (2002), analyzing *RXTE* observations of three atoll sources (Aql X-1, 4U 1608-52 and 4U 1705-44), and Muno et al. (2002), analyzing a sample of 15 LMXBs, showed that atoll sources that exhibit X–ray intensity variations by more than a factor 10 trace a Z–pattern in the CD like the Z sources and concluded that these atoll sources evolve with the mass accretion rate in similar ways to the Z sources. According to Gierliński & Done (2002), both sets of sources undergo a transition from the upper to the lower branch of the CD when the disk, which is truncated during the upper branch, penetrates down to the NS surface, but in the case of the atolls, the disk truncation is due to mass evaporation while in the case of the Z sources this is due to the NS magnetic field. However, as also pointed out by Muno et al. (2002), while the time evolution of both classes of sources could be similar, their spectral behaviour is notably different, making the unification of the two classes of sources difficult. Also, both studies did not address the timing information associated with the motion through the CD, so that their conclusion that a Z–shape is traced out is not yet entirely secure.

Among LMXBs there are still unclassified sources: on the basis of the data already available, these sources do not display any peculiarity in their X–ray light curve or X–ray colour–colour behaviour. *BeppoSAX* (Boella et al. 1997a) offers the possibility to investigate them, thanks to the broad energy band (0.1–200 keV) and high sensitivity of the Narrow Field Instruments (NFIs) onboard. We thus started an observational campaign on a sample of these LMXBs. In this paper we report results for X1543–624 and X1556–605. The paper is organized as follows: in Sect. 2 we report the present status of knowledge of X1543–624 and X1556–605, in Sect. 3 we describe our observations and the data analysis, in Sect. 4 we present the results, in Sect. 5 we discuss them and in Sect. 6 we draw our conclusions.

2. The X–ray sources X1543–624 and X1556–605

2.1. X1543–624

X1543–624 was classified by Warwick et al. (1981) as a persistent LMXB with a 2–10 keV mean flux of $\sim 7 \times 10^{-10}$ erg cm^{-2} s^{-1}, which can vary by a factor ∼2. Apparao et al. (1978) provided an accurate position of the source (error radius of 30″) with a list of candidate optical counterparts. Subsequently McClintock et al. (1978), by means of spectrophotometric measurements, found that the most likely counterpart was the object #6 of Apparao et al. (1978) (magnitude $B \gtrsim 20$), which shows a very blue colour. The corresponding X–ray to optical luminosity is $L_{\rm X}/L_{\rm opt} \sim 1.4 \times 10^3$ (Bradt & McClintock 1983), a value quite typical for LMXBs (van Paradijs & McClintock 1995). Smith et al. (1990) with IRAS discovered a far–infrared counterpart of X1543–624 having a spectral slope compatible with that of an accretion disk. No radio counterpart of the source was detected (Wendker 1995).

Singh et al. (1994, hereafter S94), using *EXOSAT* archive data, fitted the 1–20 keV source spectrum with an absorbed plus the Comptonization model ( ) by Sunyaev & Titarchuk (1980). This fit (albeit it poorly constrained the parameters of the model) yielded an hydrogen column density of $\sim 1.3 \times 10^{22}$ cm^{-2}, a temperature $kT_{\rm bb} \sim 1.6$ keV and a Comptonizing cloud with electron temperature $kT_{\rm e} \sim 37$ keV (lower limit 4 keV) and optical depth $\tau \sim 1.2$ (upper limit 4.8). These authors also found a broad iron emission line at ∼7 keV with an Equivalent Width (EW) of ∼100 eV.

Christian & Swank (1997), using *Einstein* archival data between 0.5 and 20 keV, found that the best fit, even if unsatisfactory, of the source photon spectrum was obtained with either an model with $\Gamma \sim 1.9$ and $kT_{\rm e} \sim 25$ keV or a plus thermal bremsstrahlung ( ) model, with $kT_{\rm bb} \sim 2$ keV and $kT_{\rm tb} \sim 2.4$ keV, both models being photoelectrically–absorbed. Simpler models, such as a or a or a , provided worse fits. The estimated hydrogen column density was $N_{\rm H} \sim 2.5 \times 10^{21}$ cm^{-2}, a value about 4 times lower than that found by S94, while the source unabsorbed flux was $\sim 1 \times 10^{-9}$ erg cm^{-2} s^{-1}. No evidence of emission lines was found.

More recently A2000, in the framework of an archival survey of iron K lines in LMXBs, analyzed an observation of this source performed with ASCA on August 17 1995. During the observation the 1–10 keV unabsorbed flux of the source was 1.1×10^{-9} erg cm^{-2} s^{-1}, which is consistent with that found by Christian & Swank (1997). The 0.7–10 keV source spectrum was fit with an absorbed plus model with $kT_{\rm bb} \sim 1.6$ keV, a temperature of the inner disk $kT_{\rm in} \sim 0.7$ keV and $N_{\rm H} \sim 1.4 \times 10^{21}$ cm^{-2}, which is consistent with the estimate by Christian & Swank (1997). A2000 also marginally detected an iron emission line at 6.8 keV with $EW \sim 48$ eV. A low energy emission feature near 0.7 keV was observed from this source (White et al. 1997). Juett et al. (2001, hereafter J2001), stimulated by the results obtained on 4U 0614+091 with *Chandra*, reanalyzed the *ASCA* data of X1543–624 adopting a plus model photoelectrically–absorbed by a column density $N_{\rm H}$ with Ne and O abundances free to vary in the fit. The model, even if unsatisfactory (χ^2/d.o.f. = 1542/754), was suitable to describe the emission feature at 0.7 keV with Ne/Ne$_\odot \sim 2.9$ and O/O$_\odot \sim 0.5$. Very recently Schultz (2002) analyzed archival *ASCA*, *BeppoSAX* and *RXTE* data obtained from the observations of X1543–624. For *BeppoSAX* only LECS and MECS data were considered, while for *RXTE* only PCA data were analyzed. The spectra of each of the observations were fitted with an absorbed plus model. The 2–10 keV source luminosity was observed to increase by a factor ~1.6 (from 8.6×10^{36} erg s^{-1} to $\sim 1.4 \times 10^{37}$ erg s^{-1}), with harder spectra ($kT_{\rm e}$ from ~0.5 to ~3.5 keV and τ from ~30 to $\tau \sim 10$) at higher luminosities, unlike the general behaviour of LMXB sources (see, e.g., Bloser et al. 2000). Evidence of an Fe K emission line in the higher luminosity spectra obtained during the *RXTE* observations was reported.

2.2. X1556–605

X1556–605 was classified by Warwick et al. (1981) as a persistent, irregularly variable LMXB with a 2–10 keV flux of $\sim 3 \times 10^{-10}$ erg cm^{-2} s^{-1}, with variations within a factor ~4 (Bradt & McClintock 1983). A precise celestial position (error radius of 30″) was given by Apparao et al. (1978) using a *SAS-3* observation made on June 1975. This position allowed Charles et al. (1979) to identify the optical counterpart of the source with the star #43 (also known as LU TrA) in the finding chart reported by Apparao et al. (1978) on the basis of its spectrophotometric characteristics. This object is rather blue (U–B = –0.7) and displays a He λ4686 line in emission. These features are quite common in the optical counterparts of LMXBs. The optical counterpart showed a magnitude $V \sim 19$ and H$_\alpha$, He λ4686 and N λ4640 (Bowen blend) emission lines (Motch et al. 1989, hereafter M89). These authors also found optical variability of ~0.4 mag, not correlated with the X-ray emission, on timescales of hours. Using the data of M89, the X-ray/optical luminosity ratio of the source was ~1200 (and not 180 as erroneously reported by these authors), in better agreement with the value, 2×10^3, given by Bradt & McClintock (1983). A possible photometric orbital period of 9.1 hours, a value not inconsistent with the size and characteristics of a LMXB, was found by Smale (1991) from optical V–band observations. Lastly, this source was also detected in the far–infrared with IRAS (Smith et al. 1990), while no counterpart was found at radio wavelengths (Wendker 1995).

The *Einstein* 0.5–20 keV spectral data (Christian & Swank 1997) were better described with either an absorbed model with $N_{\rm H} \sim 3.7 \times 10^{21}$ cm^{-2}, photon index $\Gamma \sim 0.58$ and $kT_{\rm e} \sim 3.3$ keV or with a plus model with $N_{\rm H} \sim 4.6 \times 10^{21}$ cm^{-2}, $kT_{\rm bb} \sim 1.6$ keV and $kT_{\rm tb} \sim 4.9$ keV, even though the fits were not completely satisfactory. M89 performed a quasi–simultaneous X–ray/optical observational campaign on this source during the years 1984/1985. The X–ray data, collected with *EXOSAT*, showed flux variations by ~20% accompanied by changes in the hardness ratio of the emission, but did not show bursts or pulsations. The photoelectrically–absorbed 0.1–10 keV X–ray spectrum was fit with either a plus model ($N_{\rm H} \sim 4 \times 10^{21}$ cm^{-2}, $kT_{\rm bb} \sim 1.3$ keV, $kT_{\rm tb} \sim 7$ keV) or with an ($N_{\rm H} \sim 3 \times 10^{21}$ cm^{-2}, $\Gamma \sim 0.7$, $kT_{\rm e} \sim 3.8$ keV), or with a model ($N_{\rm H} \sim 5 \times 10^{21}$ cm^{-2}, $kT_{\rm e} \sim 2$ keV, $\tau \sim 20$).

Notice that the estimated column density is consistent with that derived with the *Einstein* data. The source fluxes were comparable (1–10 keV flux of $\sim 4 \times 10^{-10}$ erg cm^{-2} s^{-1}) during the EXOSAT and the *Einstein* observations. No Fe K emission line was detected in the spectrum (see also Gottwald et al. 1995).

3. Observations and data analysis

X1543–624 and X1556–605 are continuously monitored with the *All Sky Monitor* (ASM) onboard RXTE. The ASM light curve of both sources in the February–April 1997 period which covers our observations is shown in Fig. 1. We observed the sources twice (see log in Table 1) with the *BeppoSAX* NFIs.

These include a Low–Energy Concentrator Spectrometer (LECS, 0.1–10 keV; Parmar et al. 1997), three Medium–Energy Concentrator Spectrometers (MECS, 1.5–10 keV; Boella et al. 1997b), a High Pressure Gas Scintillation Proportional Counter (HPGSPC, 4–120 keV; Manzo et al. 1997), and a Phoswich Detection System (PDS, 15–300 keV; Frontera et al. 1997). At the time of these observations, Unit 1 of MECS was still operative (it failed shortly thereafter, on May 6 1997), so the four pointings reported here were performed with all three MECS units. Table 1 gives the observation log along with the exposure times. During all pointings the

NFIs worked nominally and both sources were detected in all of them.

Good data were selected from intervals when the NFIs elevation angle was above the Earth limb by at least 5° and, for LECS, during spacecraft night time. The SAXDAS 2.0.0 data analysis package (Lammers 1997) was used for the processing of the LECS, MECS and HPGSPC data. The PDS data reduction was performed using the XAS package v2.1 (Chiappetti & Dal Fiume 1997). LECS and MECS spectra were extracted from a region of 8′ radius centred on the source position after proper background subtraction. For LECS and MECS we used the background measured pointing a blank–field (Fiore et al. 1999), while for HPGSPC and PDS we continuously monitored it using the rocking–collimator technique (Frontera et al. 1997). The rocking angle and attitude was suitably choosen in order to point to sky fields with no known X–ray sources in the field of view of the instruments. The spectra were rebinned leaving an oversample by a factor of 3 of the energy resolution ($FWHM$), and having a minimum of 20 counts in each bin such that the χ^2 statistics could reliably be used. Data were selected in the energy ranges where the instrument responses are better known: 0.4–4.0 keV for the LECS, 1.8–10 keV for the MECS, 8–30 keV for the HPGSPC, and 15–200 keV for the PDS. We used the package v11.0.1 (Arnaud 1996) to fit the multi–instrument spectra. In the broad–band fits, normalization factors were applied to LECS, HPGSPC and PDS spectra following the cross–calibration tests between these instruments and the MECS (Fiore et al. 1999). The normalization factor of PDS was fixed to 0.9 for both sources. An a–posteriori check showed that indeed the best fit model parameters did not undergo any significant variation changing this factor in the range from 0.75 to 0.98 as prescribed by Fiore et al. (1999). Photoelectric absorption was modeled using the cross sections implemented in (Morrison & McCammon 1983) and, when the element abundances were fixed, we used the standard values given by Anders & Grevesse (1989). Finally, we assumed a distance d = 10 kpc for both sources, as done in previous works. Actually, Christian & Swank (1997) gave a value of 4 kpc for the distance to X1556–605 on the basis of the optical photometric period measured by Smale (1991) . However, the period inferred by this author lacks confirmation. For this reason we preferred to assume the "standard" value of 10 kpc also for X1556–605. Uncertainties in the parameters obtained from the spectral fits are single parameter errors at a 90% confidence level. The values quoted in square parentheses in Table 2 are kept frozen during the fit.

4. Results

Figure 2 shows the 2–10 keV light curves of both sources during the two observations. Neither dips nor eclipses nor X–ray bursts are observed. On time scales of several hundreds of seconds, there is evidence of a moderate time variability from X1543–623, while a small flux decrease (by ~9% in the case of X1543–623 and by ~5% in the case of X1556–605) is measured from the first to the second observation.

The MECS light curves in four energy ranges, namely 1.8–3 keV, 3–5 keV, 5–6.5 keV, 6.5–10 keV, were extracted to study the CD. The soft colour was obtained from the 3–5 keV/1.8–3 keV count rate ratio, the hard colour from the 6.5–10 keV/5–6.5 keV ratio. The CDs of both sources are shown in Fig. 3. As can be seen, both the soft and hard colours of X1543–623 and X1556–605 change by about 20% during the observations, with an almost circular pattern traced by the sources. In the case of X1543–623 the soft colour (x axis) has a centroid value of ~0.95 and the hard colour (y axis) of ~0.55, in the case of X1556–605 the hard colour has a centroid value similar to that of X1543–624, while the soft colour has a higher centroid (~1.1).

4.1. Spectral properties

As already said in Sect. 1, several models have been proposed to fit the spectra of both Z and atoll sources. In the cases of low luminosity sources, a single component model has sometimes provided good results (e.g., White et al. 1988). We thus performed our analysis first with a single component model and then with two–component models both in their "classical" forms (White et al. 1986; White et al. 1988; Mitsuda et al. 1984; Mitsuda et al. 1989) and in the forms proposed more recently (see references in Sect. 1).

4.1.1. X1543–624

We first tried photoelectrically–absorbed (in) single component models: a simple , an and the Comptonization models and . None of them was found to provide a satisfactory description of the data (χ^2_ν always higher than 4). Thus we concentrated on two–component models. The plus model provided χ^2/d.o.f. = 288/133 and 367/133 in the first and second observation, respectively, with residuals to the model sinusoidally distributed along the entire energy band. Also the plus did not give a good description of the data (χ^2/d.o.f. = 352/134 and 335/134 for the first and second observation, respectively), but, in this case, apart from an excess count around 0.7 keV, the residuals are mainly concentrated above 15 keV (see Fig. 4). Replacing the simple with a Comptonized (in ; Nishimura et al. 1986) we obtained a much better description of the data (χ^2/d.o.f. = 180/132 for the first observation and χ^2/d.o.f. = 175/132 for the second one), with the residuals to the model only at about 0.7 keV (see Fig. 5). Other two-component models used for LMXBs, like a or plus a , did not provide better fits to the data.

As noticed above, irrespective of the adopted model, positive residuals are present in both observations around 0.7 keV. Assuming as input model the plus , which gives the best fit to the continuum spectrum, these residuals can be fit either adding a Gaussian (χ^2/d.o.f. = 161/129 and 129/129 in the first and second observation, respectively), or, following J2001, assuming an absorption with free abundances of O/O$_\odot$ and Ne/Ne$_\odot$ (model in XSPEC, χ^2/d.o.f. = 160/130 and 131/130, in the first and second observation, respectively).

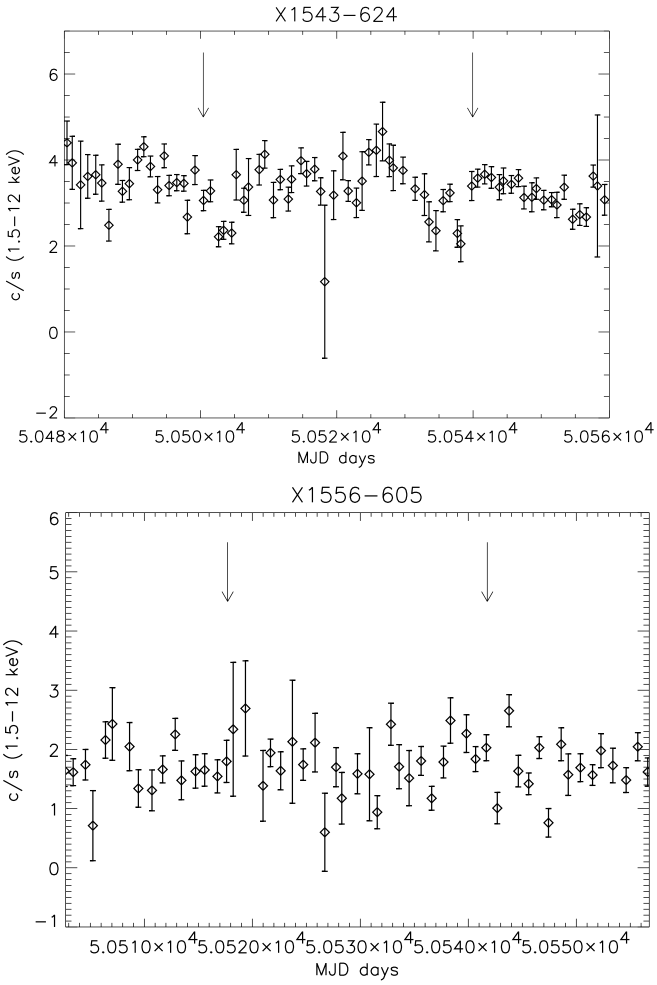

Fig. 1. The one day average light curves of X1543–624 and X1556–605 detected with the *RXTE* ASM in the 1.5–12 keV energy band. The arrows mark the epoch of the *BeppoSAX* observations of each source. ASM data can be retrieved on the public archive at `http://xte.mit.edu/XTE/asmlc/ASM.html`

The Gaussian centroid energy (∼0.65 keV) is consistent with fluorescence emission from O or O , and the abundances of O and Ne, assuming the model, are reported in Table 2. For the reasons discussed by J2001 we prefer the interpretation of the 0.7 keV excess in terms of absorption in neon–rich material local to the binary.

Stimulated by the residuals in the 5–10 keV energy range during the first observation (see Fig. 5), we investigated the presence of Fe K emission lines and/or K edges. Assuming for the emission line a Gaussian profile $(I_l/(\sqrt{2\pi}\sigma_l) \times \exp[-(E-E_l)^2/2\sigma_l{}^2])$, with centroid energy E_l in the range from 6.4 to 6.9 keV the best fit was obtained with $E_l = 6.4$ keV, with a decrease in the χ^2/d.o.f. from 160/130 to 150/128 (significance level of ∼1%) in the first observation and from 131/130 to 125/128 (significance level of ∼5%) in the second observation. The best fit parameter values of the line are reported in Table 2. We note that these values are marginally consistent with those obtained by S94 and A2000. The $EF(E)$ unabsorbed spectrum of the source with its best fit model, components and residuals of the data to the model is shown in Fig. 7 for both observations.

Adding an absorption edge in both observations did not improve the fit and the optical depth is consistent with zero. As can be seen from Table 2, the best fit values of $N_{\rm H}$ in the two observations are marginally consistent with each other and with the Galactic value obtained from the radio data along the source direction (3×10^{21} cm^{-2}, Dickey & Lockmann 1990).

The source X–ray unabsorbed luminosity in various energy bands is shown in Table 2. While the 1–20 keV luminosity shows a very slight decrease (∼10%) from the first to the second observation, the partially extrapolated 20–200 keV luminosity increases by a factor of about 2.

4.1.2. X1556–605

Given the lower statistical quality of the spectra of X1556–605 (see count rate from the source in Table 1), the spectral analysis of the single observations could not be as detailed as in the case of X1543–624. The count rate spectra of the two observations, within their uncertainties, were consistent with each other, so we performed the spectral analysis on the average spectrum. A photoelectrically–absorbed is unable to describe the data ($\chi^2_\nu > 10$). Models with a high–energy cut–off (and in order to compare our results with those obtained by M89) are still unsatisfactory (with χ^2/d.o.f. = 160/126, while with χ^2/d.o.f.=183/126), but the best fit parameter values are very similar to those obtained by M89. The photoelectrically–absorbed two–component model plus also leaves a significant excess above 15 keV (χ^2/d.o.f. = 156/125, see Fig. 6); instead the photoelectrically–absorbed plus or plus give satisfactory descriptions of the data (χ^2/d.o.f. = 141/124 and 134/123, respectively). The unabsorbed $EF(E)$ model spectra and the residuals to the models are shown in Fig. 8, while the best fit parameters are reported in Table 2.

The derived $N_{\rm H}$ is in agreement with the Galactic column density $N_{\rm H} = 0.3 \times 10^{22}$ cm^{-2} along the source direction derived from radio maps (Dickey & Lockmann 1990) and with the value (0.27×10^{22} cm^{-2}) derived from the extinction $E_{B-V} = 0.55$ of the optical counterpart by M89, adopting the E_{B-V} vs. $N_{\rm H}$ relation by Diplas & Savage (1994). We find no evidence of emission lines in the spectrum. The luminosities in the same energy ranges adopted for X1543–624 are reported in Table 2. As can be seen, the source luminosity derived with the two models are similar in the 1–20 keV energy band. However, the partially extrapolated 20–200 keV luminosity is model dependent: it is higher in the case of plus than in the case of plus .

4.2. Timing properties

No periodicity down to ∼10 ms time scale can be inferred from the power spectral density (PSD) estimate of the 2–10 keV light curves (MECS data) of the two sources. The PSD, evaluated in ∼10^{-3}–10 Hz frequency range, do not show statistically significant fractional variations of the source fluxes: in the case of X1543–623 the upper limit at 95% confidence level is ∼9% in the first observation and 12% in the second one, in the case of

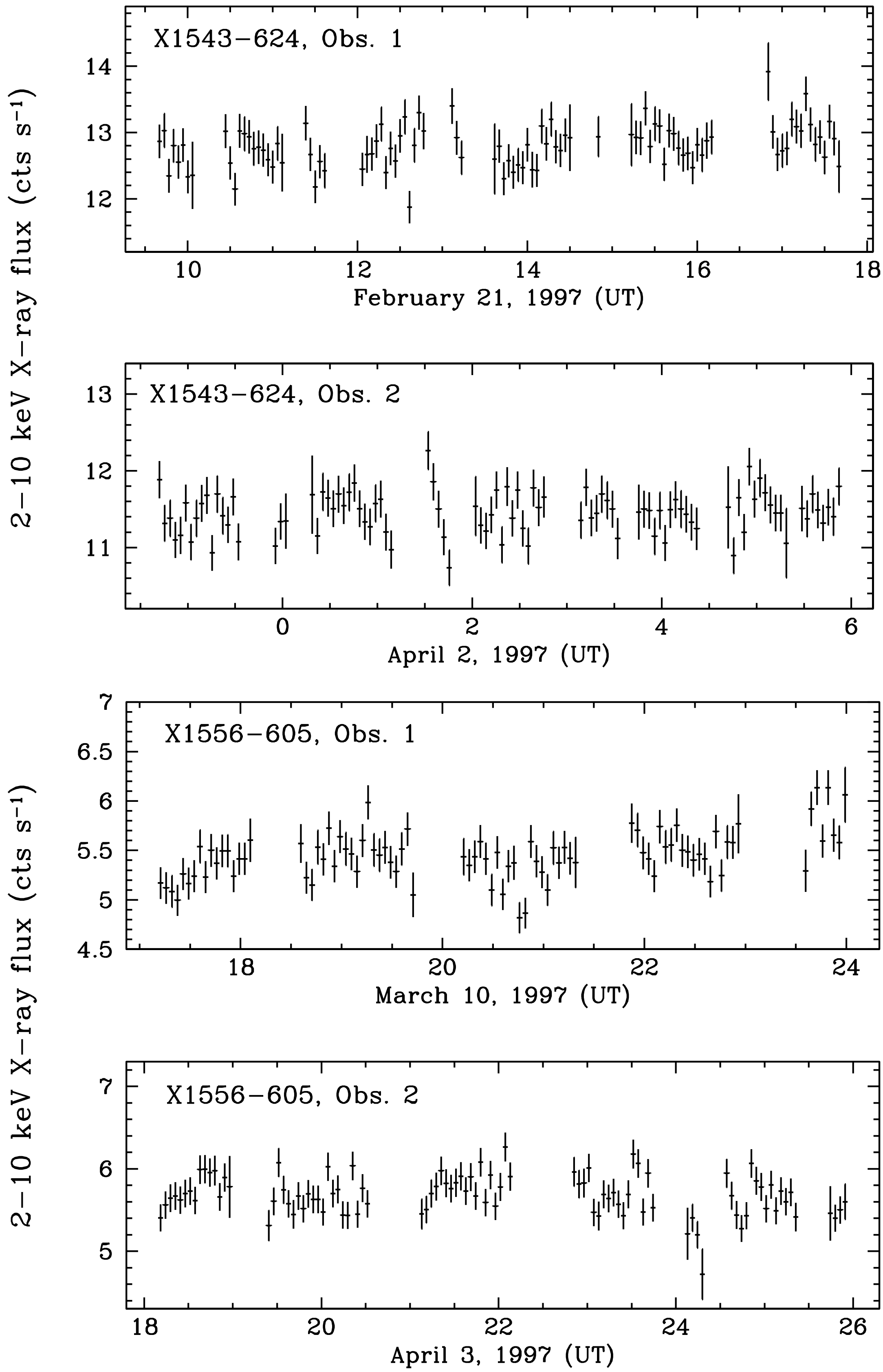

Fig. 2. *Upper panels:* 2–10 keV MECS light curves of the two *BeppoSAX* observations of X1543–624. *Bottom panels:* 2–10 keV MECS light curves of X1556–605. Times are expressed in UT of the day reported in each panel. The time binning is 200 s.

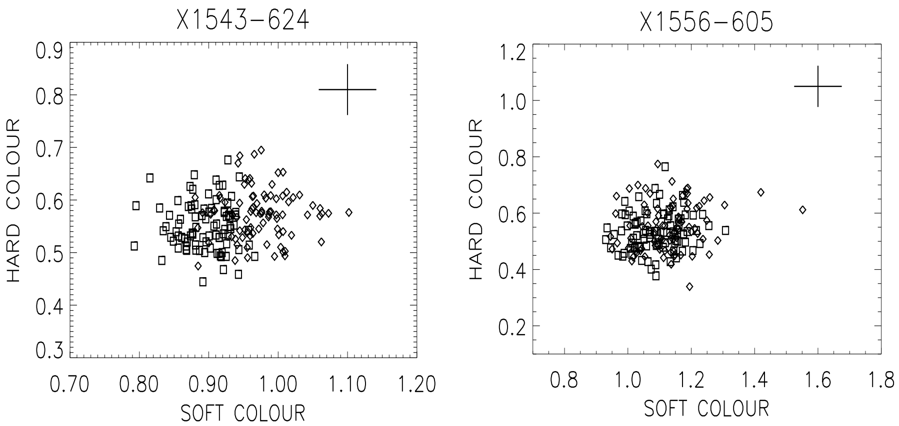

Fig. 3. Colour–colour diagrams of both observations of X1543–624 (*left panel*) and X1556–605 (*right panel*). The y axis (*hard colour*) gives the ratio between the 6.5–10 keV and 5–6.5 keV count rates. The x axis (*soft colour*) gives the count rate ratio in the 3–5 keV and 1.8–3 keV energy bands. In both diagrams each point corresponds to a time interval of 200 s. Typical error bars of the two colours are reported in the top right of each panel. *Diamonds*: first observation; *squares*: second observation.

Table 2. Best fit continuum parameters of the observed LMXBs.

	X1543–624		X1556-605	
Parameter	Obs. 1	Obs. 2	Obs. 1+2	
	(+	+)	(+)	(+)
N_H^a	$0.21^{+0.04}_{-0.03}$	$0.31^{+0.02}_{-0.06}$	$0.30^{+0.01}_{-0.02}$	$0.37^{+0.03}_{-0.06}$
kT_{bb} (keV)	$1.45^{+0.01}_{-0.01}$	$1.44^{+0.01}_{-0.01}$	$1.49^{+0.03}_{-0.02}$	$1.49^{+0.23}_{-0.09}$
kT_e (keV)	$6.7^{+1.5}_{-0.7}$	$25.4^{+5.2}_{-4.3}$	$17.5^{+12.6}_{-8.4}$	$4.1^{+0.5}_{-0.8}$
τ	$1.3^{+0.1}_{-0.1}$	$0.5^{+0.1}_{-0.1}$	$0.5^{+0.2}_{-0.1}$	–
Γ	–	–	–	$1.0^{+0.2}_{-0.3}$
kT_{in} (keV)	$0.64^{+0.01}_{-0.01}$	$0.62^{+0.02}_{-0.02}$	$0.93^{+0.06}_{-0.05}$	–
$R_{in}\sqrt{\cos(i)}$ or R_{bb} (km)	$14.1^{+1.0}_{-0.8}$	$16.2^{+1.1}_{-1.1}$	$3.9^{+0.4}_{-0.4}$	$1.2^{+0.2}_{-0.5}$
L^b_{dbb} or L^b_{bb}	8.6	9.7	2.9	1.1
E_l (keV)	[6.4]	[6.4]	–	–
σ_l (keV)	$0.7^{+0.4}_{-0.4}$	$0.7^{+1.1}_{-0.7}$	–	–
I_l (10^{-4} cm^{-2} s^{-1})	$5.3^{+4.7}_{-3.1}$	$3.8^{+10.8}_{-3.1}$	–	–
EW_l (eV)	65^{+58}_{-39}	55^{+159}_{-45}	–	–
O/O$_\odot$	$0.32^{+0.26}_{-0.27}$	<0.33	–	–
Ne/Ne$_\odot$	$2.4^{+0.5}_{-0.7}$	$2.8^{+1.0}_{-0.6}$	–	–
χ^2/d.o.f.	150/129	125/129	134/124	141/124
$L^b_{0.1-200\ keV}$	18.9	18.6	6.8	7.2
$L^b_{1-20\ keV}$	15.0	13.8	5.8	5.9
$L^b_{20-200\ keV}$	0.3	0.6	0.14	0.05

[a] In units of 10^{22} cm^{-2}.
[b] Unabsorbed luminosity in units of 10^{36} erg s^{-1} assuming a distance of 10 kpc for both sources.

X1556–605 the upper limit at 95% confidence level is 14% in the first observation and 16% in the second one.

5. Discussion

It is the first time that two unclassified LMXB sources, X1543–624 and X1556–605, have been deeply investigated in a broad energy band (0.4–200 keV) with two observations separated by about one month. The first source was detected up to 50 keV and the other up to 25 keV. Both sources show many similar properties. We discuss now the implications of these properties.

5.1. Source nature and classification

The spectrum of both X1543–624 and X1556–605 can be described by a two–component model consisting of a soft component ( ), likely coming from a cool accretion disk, plus a hard component provided by the Comptonization of a .

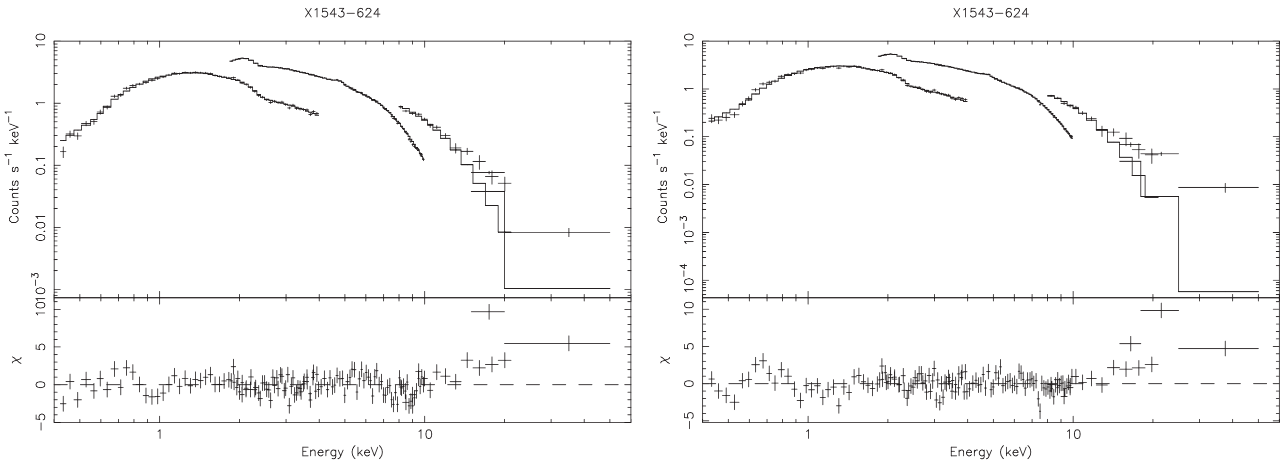

Fig. 4. Count rate spectra of the two observations of X1543–624 along with the folded model plus , photoelectrically–absorbed ( ) and residuals to the model in units of σ. *Left panel*: first observation. *Right panel*: second observation. The excess above 15 keV can be recovered replacing the with a Comptonized (see text).

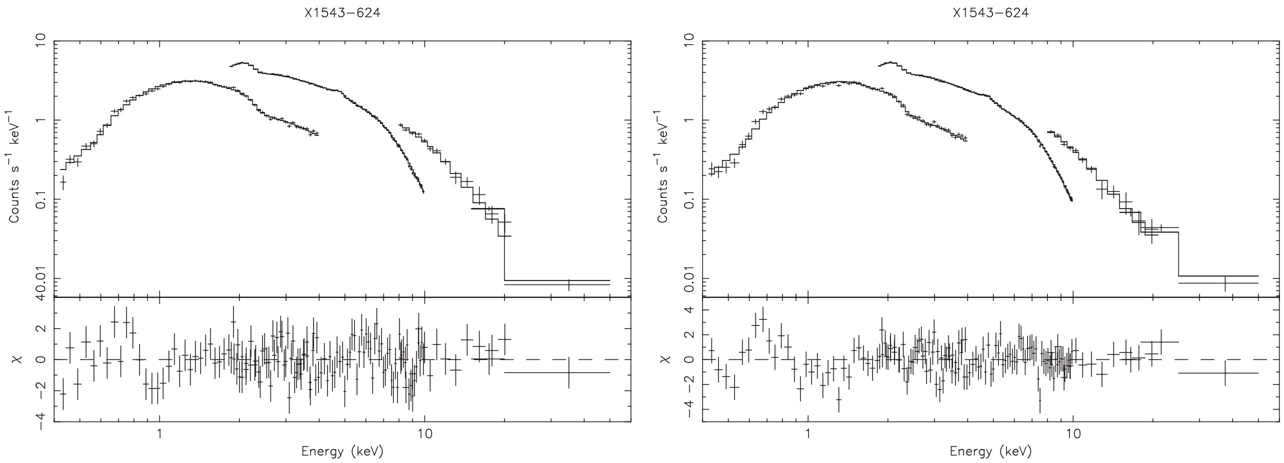

Fig. 5. Count rate spectra of the two observations of X1543–624 along with the folded model plus , photoelectrically–absorbed ( ) and residuals to the model in units of σ. *Left panel*: first observation. *Right panel*: second observation.

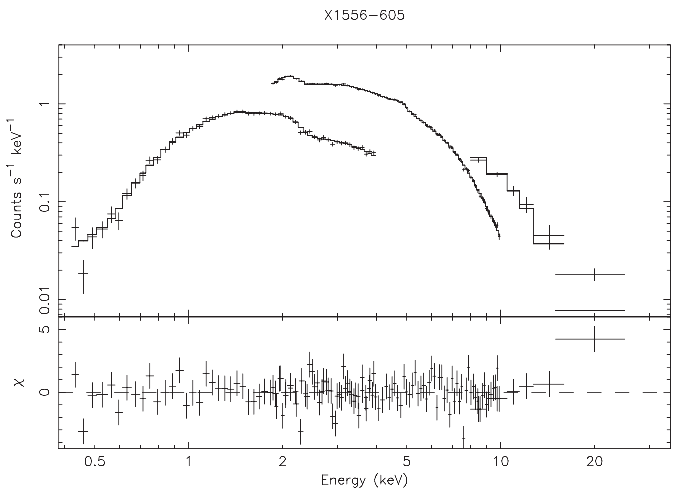

Fig. 6. *Top panel*: average count rate spectrum of the two observations of X1556–605 and best fit folded model consisting of a plus a photoelectrically–absorbed ( ). *Bottom panel*: residuals to the model in units of σ. The excess above 15 keV can be recovered either replacing the with a Comptonized or replacing the with an model (see text).

The temperature $kT_{\rm bb}$ of both sources is ~1.5 keV, while their temperature $kT_{\rm in}$ ranges from ~0.6 to ~0.9 keV. Both $kT_{\rm bb}$ and other parameters of the model ($kT_{\rm e}$, $R_{\rm in}\sqrt{\cos(i)}$) are in the range of values generally found for LMXBs containing a low–magnetic field NS. Only the best fit value of τ ($\lesssim$1), for both sources, is lower than the typical range of values (5–15) found for this class of sources (see review by Barret 2001). However the best fit value of this parameter is model dependent (e.g., we find $\tau > 10$ for a plus model). All that strongly points to a NS nature of both X1543–624 and X1556–605. The projected inner disk radius obtained for X1543–624 is consistent with this conclusion, while a very small value (~4 km) is found for X1556–605. However, small values of the projected inner disk radius have been found in other weakly magnetized accreting NS (e.g., 2.8 km for GX3+1, Oosterbroek et al. 2001). Actually the *effective* inner disk radius (Shimura & Takahara 1995; Merloni et al. 2000) is given by $R_{\rm eff} \sim R_{\rm in} \times f_{\rm col}^2$, where $f_{\rm col}$ is the spectral hardening factor. As discussed by Shimura & Takahara (1995), for luminosities down to ~0.1 times the Eddington luminosity, the conventional value $f_{\rm col} = 1.7$ can be adopted. This condition can be applied to X1543–624 ($L_{0.1-200\ \mathrm{keV}} \sim 0.1 \times L_{\mathrm{Edd}}$, see below), finding $R_{\mathrm{eff}} \sim 60$ km for a disk inclination angle $i = 60°$ (the source does not show dips or eclipses) and, marginally, for X1556–605 ($L_{0.1-200\ \mathrm{keV}} \sim 0.05 \times L_{\mathrm{Edd}}$ for a distance of 10 kpc, see below), finding $R_{\mathrm{eff}} \sim 16$ km for the same disk inclination angle.

A common property of our sources is their flux and spectrum stability. From the ASM data archive[1] one can see that both sources show intensity variations not greater than a factor of 2 on time scales of months. As shown in Table 2, the parameter values of the best fit spectrum of X1543–624 also do not change from the first to the second observation, except the plasma electron temperature kT_{e} which increases from ~7 to ~25 keV. The spectra obtained in the two observations of X1556–605 are consistent with each other, as discussed in Sect. 4.1.2. On longer time scales the source spectra appear stable: when we adopted the same models used to describe the source spectra obtained in the previous observations (a plus for X1543–624, A2000; a simple or for X1556–605, M89) the fits, even if unsatisfactory, provided similar parameter values.

The spectral stability of both sources is also apparent from their CD (see Fig. 3), which is unlike those of traditional Z sources, which show spectral variations on time scales of hours to days. Both the soft and hard colours change by about 20%, an extent consistent with that exhibited by atoll sources in their banana branch. The CD shape is similar to that of atoll sources with low flux variations ($F_{\mathrm{max}}/F_{\mathrm{min}} < 10$) (Muno et al. 2002). A similar CD pattern is shown, e.g., by the X–ray burster GS1826–238, which also exhibits intensity variations within a factor of 2 (Muno et al. 2002). The only difference we find with GS1826–238 is in the centroid value of the hard colour, which in the latter source is significantly higher (~1.5), as found with *BeppoSAX* (Del Sordo et al. 2003).

The luminosity of X1543–624 and X1556–605 supports an atoll classification. In the case of X1543–624, the average bolometric luminosity (0.1–200 keV) is $L_X \sim 2 \times 10^{37}(d/10\ \mathrm{kpc})^2$ erg s^{-1}, which corresponds to $\sim 0.1 \times L_{\mathrm{Edd}}$ (the Eddington luminosity is $L_{\mathrm{Edd}} = 1.48 \times 10^{38} M/M_{\odot}$ erg s^{-1} if an H mass fraction $f_{\mathrm{H}} = 0.7$ and a NS mass of 1.4 $M_{\odot}$ is assumed), and, in the case of X1556–605 it is $L_X \sim 7 \times 10^{36}(d/10\ \mathrm{kpc})^2$ erg s^{-1} corresponding to $\sim 0.05 \times L_{\mathrm{Edd}}$. Both luminosities are typical of X–ray bursters (see e.g., Barret et al. 2000, hereafter B2000).

We have also checked the atoll assumption using the luminosity comparison criterion first introduced by Barret et al. (1996). In Fig. 9 we show the hard X–ray (20–200 keV) luminosity versus the soft X–ray (1–20 keV) luminosity not only for the X–ray bursters and BHCs candidates listed by B2000, but also for Z sources during their exhibition of hard tails (see Sect. 1), for a new transient BHC (XTE J1118+480, Frontera et al. 2001), and for two additional atoll sources, 4U1728–34 and 4U1820–30, both detected up to 100 keV, the first with *BeppoSAX* (Di Salvo et al. 2000b), the second with RXTE (Bloser et al. 2000) in both the "island" and upper "banana" states. As can be seen, X1543–624 and X1556–605 are both in the *X–ray burster box* introduced by Barret et al. (1996), but this fact does not help to constrain the source class. Indeed, from one side, XTE J1118+480 is inside this box, while, on the other side, an atoll, 4U1820–30, is outside the box in both the island and banana states, moreover in positions which are indistinguishible from Z sources with hard tails and from some of BHCs. Note that also the Z sources Cyg X-2 (Kuulkers et al. 1995) and GX17+2 (Sztajno et al. 1986; Kuulkers et al. 1997) are X–ray bursters, and are outside the X–ray burster box.

If X1543–624 and X1556–605 are atolls, the absence of broad–band noise, as found from the PSD estimate, would be in favour of a banana state for these sources.

An open question is the absence of X–ray bursts from the two sources, which would definitively confirm the NS nature of the compact object. However the fact that bursts have not been observed does not imply that they do not occur; there is still not an extensive coverage of both X1543–624 and X1556–605 (either with *BeppoSAX* or with other satellites), so bursts can be easily missed, especially if both sources have low burst recurrence. In fact there are sources which, even though they have been known for many years, only recently have shown X–ray bursts (SLX 1737–282, in 't Zand et al. 2002; 2S 1711–339, Cornelisse et al. 2002). In the case of X1543–624, an unusual composition of the companion might lead to atypical burst properties, such as very long recurrence times (>0.5 yr for thermonuclear flashes in pure C layers) and corresponding large fluences (Joss & Li 1980). Three of the four sources analyzed by J2001 (4U 0614+091, Swank et al. 1978, Brandt et al. 1992; 2S 0918-549, Jonker et al. 2001; 4U 1850–087, Hoffman et al. 1980) have shown burst properties which induced the authors to exclude the possibility of the donor being a C–O dwarf. However we suggest that the conclusion of J2001 cannot be extended to X1543–624, because this source, unlike the three sources mentioned above, still has not shown X–ray bursts whose properties could exclude a C–O dwarf nature of the companion. In the case of X1556–605, the burst absence (or recurrence on very long time scales) could be due to an underabundance of CNO, which was observed in this source by M89. CNO is an important parameter which determines the rate at which hydrogen burns into helium (Hoyle & Fowler 1965) and therefore the recurrence time of X–ray bursts (Fujimoto et al. 1987). Moreover in X1556–605 the accretion rate is low, as inferred by its X–ray luminosity. Wallace et al. (1982) have shown that low metallicity in conjunction with a low accretion rate favours the long interval between bursts and very energetic thermonuclear runaways, and this could be the case of X1556–605 (M89).

5.2. Accretion geometry

Including the corrections for the spectral hardening factor we found that the inner disk radius of X1543–624 should be at ~5 NS radii. A likely explanation of this result, taking into account the low magnetic field of the source class to which

[1] ASM archive is available by internet at
`http://xte.mit.edu/XTE/asmlc/ASM.html`

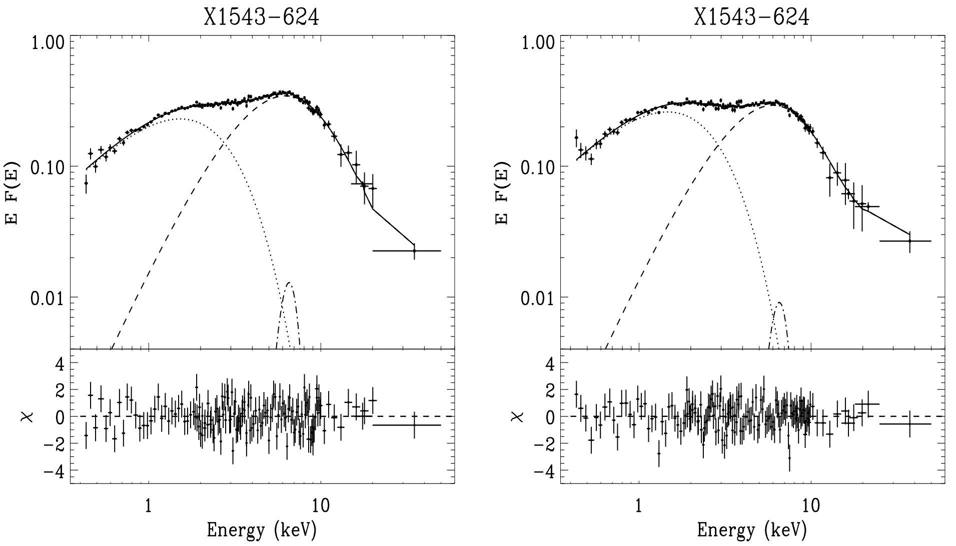

Fig. 7. Absorption–corrected, $EF(E)$ spectra for the first (*left panel*) and second (*right panel*) observation of X1543–624 with superimposed the best fit model composed by a (*dotted line*) plus (*dashed line*) plus a Gaussian (*dotted–dashed line*) at 6.4 keV (see text). *Bottom panels*: residuals, in units of σ, to the best fit model photoelectrically–absorbed with non–standard values of O and Ne ( ).

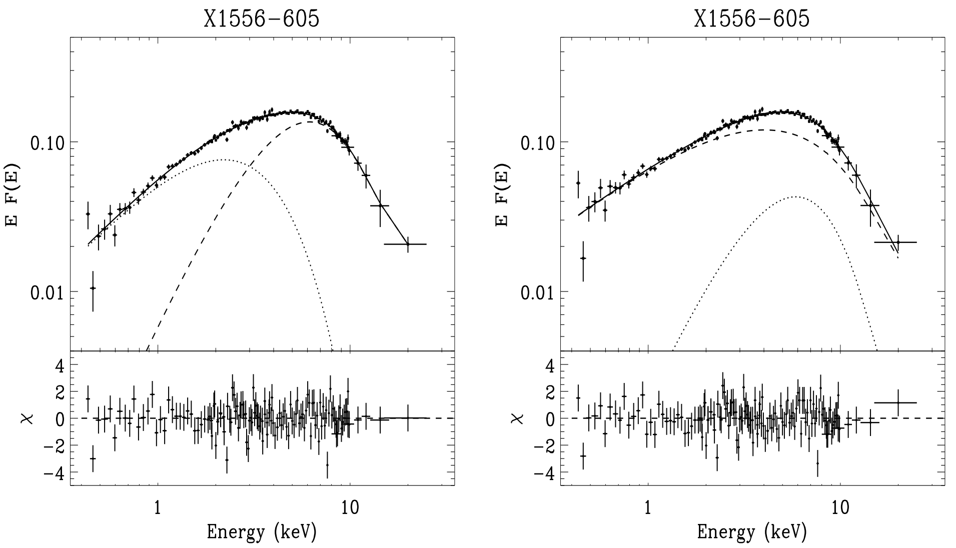

Fig. 8. Same as in Fig. 7 but for the time averaged spectrum of X1556–605. *Left panel*: (*dotted line*) plus (*dashed line*). *Right panel*: (*dotted line*) plus (*dashed line*). *Bottom panels*: residuals, in units of σ, to the best fit models, photoelectrically–absorbed ( ).

X1543–624 belongs, is that the inner accretion disk is replaced by an optically thin hot accretion flow, following the scenario suggested by B2000 on the basis of the spectral properties of a sample of bursters studied with *RXTE*. Optically thin hot accretion flows (the *Advection Dominated Accretion Flows*, ADAF) have been demonstrated (Narayan & Yi 1995) to be stable and preferrably occur at relatively low accretion rates (such as in the case of X1543–624) and this scenario strengthens the atoll hypothesis for this source. One controversial point is that the spectrum hardens (as testified by the significant increase of $kT_{\rm e}$, see Table 2) despite the fact that the luminosity increases, while the 0.1–200 keV luminosity remains constant. Another anomalous behaviour has also been noticed by Schultz (2002), as discussed in Sect. 2.1: a spectral hardening as the source luminosity increases. The reason for this different behaviour is unclear and could be connected to a quite complex geometry of the accretion flow.

In the case of X1556–605, the inner disk radius, once corrected for the spectral hardening factor, is consistent with being close to the NS surface, so that for this source the ADAF scenario appears less suitable. On the other hand, on the basis of the above considerations, it is unclear why the ADAF scenario should occur in X1543–624 and not in X1556–605, which is less luminous and thus is expected to have a lower accretion rate. However, given that the X–ray spectrum of X1556–605 can be also described by a plus (Western model), another accretion scenario can be considered for this source, in which the soft component (with $kT_{\rm bb} \sim 1.5$ keV) arises from the NS surface (or the boundary layer) and the hard component is due to Comptonization of the radiation from the inner disk. In this scenario the small radius derived ($\sim$1 km, see Table 2) could be ascribed to non–isotropic emission from the NS, as in the case of emission coming from an equatorial belt

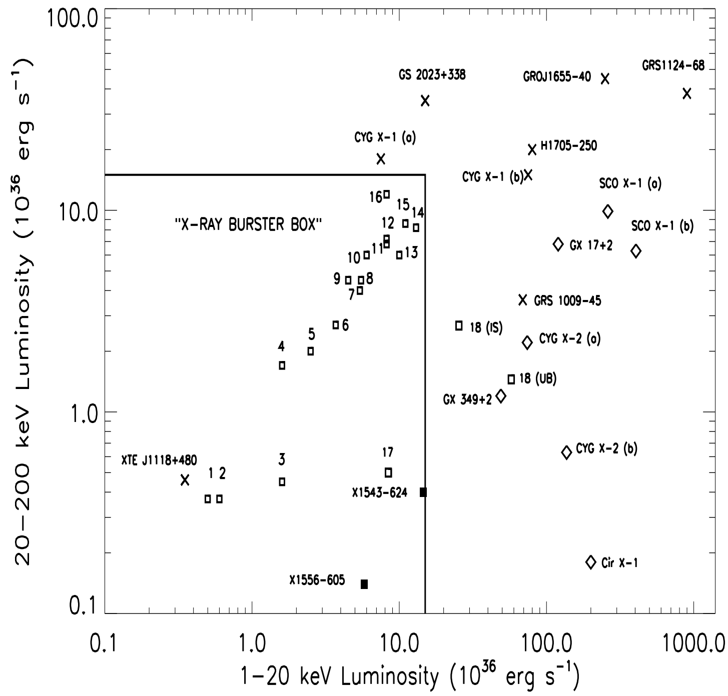

Fig. 9. The hard (20–200 keV) X–ray luminosity versus the soft (1–20 keV) luminosity for weakly magnetic compact X–ray binaries. *Open squares*: X-ray bursters detected up to 100 keV and listed in the analoguous figure by B2000; *open diamonds*: Z sources; *crosses*: black holes candidates. The *"X–ray burster box"* introduced by B2000 is also shown. BHCs are mostly located on the right, but one of them (XTE J1118+480) is inside the X–ray burster box. The position of our two sources (*filled squares*) within the X–ray burster box is shown. The points (*a*) and (*b*) for Sco X–1 denote the minimum and maximum fluxes observed by D'Amico et al. (2001) during their detection of a hard tail; the points (*a*) and (*b*) for Cyg X–2 denote the cases in which the the hard X–ray tail was detected and not detected, respectively (Di Salvo et al. 2002). The points (*a*) and (*b*) for Cyg X–1 denote the low/hard state and the high/soft state, respectively. The numbers from 1 to 16 denote the X–ray bursters listed by B2000, while 17 and 18 denote two additional atoll sources included in the figure; 1: Aql X–1; 2: SLX1732–304; 3: 4U0614+09; 4: XB1323–619; 5: SAXJ1808.4–3658; 6: 4U1915–05; 7: SLX1735–269; 8: A1742–294; 9: 4U1608–52; 10: SAXJ1748.9–2021; 11: 1E1724–3045; 12: GS1826–238; 13: KS1731–260; 14: GX354–0; 15: Cen X–4; 16: 4U1705–44; 17: 4U1728–34 (Di Salvo et al. 2000b); 18: 4U1820-30 (Bloser et al. 2000).

(Inogamov & Sunyanev 1999), or to the fact that the plasma responsible for the Comptonization of the radiation from the inner disk also intercepts part of the flux coming from the NS surface, thus reducing the flux and hence its radius.

The evidence of an Fe K emission line from X1543–624, with the energy centroid of the line at 6.4 keV, suggests fluorescence emission from a neutral medium, such as from a disk not extending down to the NS surface, in agreement with the above considerations. However the non–detection of an Fe K line from X1556–605 remains unclear if the disk extends down to the NS surface.

6. Conclusions

From the above discussion it emerges that X1543–624 and X1556–605 show properties of atolls in the banana state, even if the shape of the CD is not strictly reminiscent of a banana. However it is similar to the CD of atoll sources with small intensity variations (e.g., GS1826−238). The high $L_{1-20\,\mathrm{keV}}/L_{20-200\,\mathrm{keV}}$ ratio is also found in atoll sources (see Fig. 9). The absence of type I X–ray bursts may be explained by their long recurrence times and by the short observation times of the two sources. The accretion geometry of X1543–624 is consistent with that of sources inside the X–ray burster box, for which an ADAF scenario appears suitable to describe their spectral behaviour (B2000). X1543–624 shows, in addition to an Fe K emission line, a stable emission feature at ~0.7 keV, which is likely due to the K edges of local O and Ne with non–solar abundances, as found for other sources (J2001). Even in this case X–ray bursts, although with atypical properties and frequencies, should be expected, but they have not been observed until now. For X1556–605 both the scenarios proposed by the Western and Eastern models are possible, and on the basis of our data we cannot decide which of them is preferrable. A broad–band, long and more sensitive monitoring could be of key importance to better understand these LMXBs and to better constrain the mass accretion scenario.

Acknowledgements. Many thanks to the anonymous referee for the very useful suggestions and comments on the first version of our paper. This research is supported by the Italian Space Agency (ASI) and Ministry of University and Scientific Research of Italy (COFIN funds). *BeppoSAX* is a joint Italian and Dutch program.

References

Anders, E., & Grevesse, N. 1989, Geochim. Cosmochim. Acta, 53, 197

Apparao, K. M. V., Bradt, H. V., Dower, R. G., et al. 1978, Nature, 271, 225

Arnaud, K. A. 1996, XSPEC: the first ten years, in Proceedings of the V ADASS Symposium, ed. G. H. Jacoby, & J. Barnes, ASP Conf. Ser., 101, 17

Asai, K., Dotani, T., Nagase, F., & Mitsuda, K. 2000, ApJS, 131, 571 (A2000)

Asai, K., Dotani, T., Mitsuda, K., et al. 1994, PASJ, 46, 479

Barret, D., McClintock, J. E., & Grindlay, J. E. 1996, ApJ, 473, 963

Barret, D., Olive, J. F., Boirin, L., et al. 2000, ApJ, 533, 329 (B2000)

Barret, D. 2001, AdSpR, 28, 307

Bloser, P. F., Grindlay, J. E., Kaaret, P., et al. 2000, ApJ, 542, 1000

Boella, G., Butler, R. C., Perola, G. C., et al. 1997a, A&AS, 122, 299

Boella, G., Chiappetti., L., Conti., G., et al. 1997b, A&AS, 122, 327

Bradt, H. V., & McClintock, J. E. 1983, ARA&A, 21, 13

Brandt, S., Castro–Tiraldo, A. J., Lund, N., et al. 1992, A&A, 262, L15

Charles, P. A., Thorstensen, J. R., Bowyer, S., et al. 1979, BAAS, 11, 720

Chiappetti, L., & Dal Fiume, D. 1997, in Proceedings of the Fifth International Workshop on Data Analysis in Astronomy, System, ed. V. di Gesù, M. J. B. Duff, A. Heck, M. C. Maccarone, L. Scarsi, & H. U. Zimmermann (World Scientific Press), 101

Christian, D. J., & Swank, J. H. 1997, ApJS, 109, 177

Cornelisse, R., Verbunt, F, in 't Zand, J. J. M., et al. 2002, A&A, 392, 885

D'Amico, F., Heindl, W. A., Rothschild, R. E., et al. 2001, ApJ, 547, L147

Del Sordo, S., et al. 2003, in preparation

Dickey, J. M., & Lockmann, F. J. 1990, ARA&A, 28, 215

Diplas, A., & Savage, B. D. 1994, ApJ, 427, 274

Di Salvo, T., Stella, L., Robba, N. R., et al. 2000a, ApJ, 544, L119

Di Salvo, T., Iaria, R., Burderi, L., & Robba, N. R. 2000b, ApJ, 542, 1034

Di Salvo, T., Robba, N. R., Iaria, R., et al. 2001, ApJ, 554, 49

Di Salvo, T., Farinelli, R., Burderi, L., et al. 2002, A&A, 386, 535

Fiore, F., Guainazzi, M., & Grandi, P. 1999, Technical Report 1.2, *BeppoSAX* scientific data center, available online at `ftp://www.sdc.asi.it/pub/sax/doc/software_docs/saxabc_v1.2.ps`

Frontera, F., Costa, E., Dal Fiume, D., et al. 1997, A&AS, 122, 357

Frontera, F., Dal Fiume, D., Malaguti, G., et al. 1998, in The Active X–ray Sky, ed. L. Scarsi, H. Bradt, P. Giommi, & F. Fiore, Nucl. Phys. B, 69, 286

Frontera, F., Zdziarski, A. A., Amati, L., et al. 2001, ApJ, 561, 1006

Fujimoto, M. Y., Sztajno, M., Lewin, W. H. G., et al. 1987, ApJ, 319, 902

Gierliński, M., & Done, C. 2002, MNRAS, 331, L47

Gottwald, M., Parmar, A. N., Reynolds, A. P., et al. 1995, A&AS, 109, 9

Harmon, B. A., Wilson, C. A., Tavani, M., et al. 1996, A&AS, 120, 197

Hasinger, G., & van der Klis, M. 1989, A&A, 225, 79

Hoffman, J. A., Cominsky, L., & Lewin, W. H. G. 1980, ApJ, 240, L27

Hoyle, F., & Fowler, W. A. 1965, in Quasi–stellar Sources and Gravitational Collapse, ed. I. Robinson, A. Schild, & E. L. Shucking (Chicago: University of Chicago Press), 17

Iaria, R., Burderi, L., Di Salvo, T., et al. 2001, ApJ, 547, 412

in 't Zand, J. J. M., Verbunt, F., Kuulkers, E., et al. 2002, A&A, 389, L43

Inogamov, N. A., & Sunyaev, R. A. 1999, AstrL, 25, 269

Jonker, P. G., Peter, G., van der Klis, M., et al. 2001, ApJ, 553, 335

Joss, P. C., & Li, F. K. 1980, ApJ, 238, 287

Juett, A. M., Psaltis, D., & Chakrabarty, D. 2001, ApJ, 560, 59 (J2001)

Kuulkers, E., van der Klis, M., & van Paradjis, J. 1995, ApJ, 450, 748

Kuulkers, E., van der Klis, M., Oosterbroek, T., et al. 1997, MNRAS, 287, 495

Lammers, U. 1997, The SAX/LECS Data Analysis System User Manual, SAX/LEDA/0010

Manzo, G., Giarrusso, S., Santangelo, A., et al. 1997, A&AS, 122, 341

McClintock, J. E., Canizares, C., Hiltner, W. A., & Petro, L. 1978, IAU Circ., 3251

Merloni, A., Fabian, A. C., & Ross, R. R. 2000, MNRAS, 313, 193

Mitsuda, K., Inoue, H., Koyama, K., et al. 1984, PASJ, 36 741

Mitsuda, K., Inoue, H., Nakamura, N., & Tanaka, Y. 1989, PASJ, 41, 97

Morrison, R., & McCammon, D. 1983, ApJ, 270, 119

Motch, C., Pakull, M. W., Mouchet, M., & Beuermann, K. 1989, A&A, 219, 158 (M89)

Muno, M. P., Remillard, R. A., & Chakrabarty, D. 2002, ApJ, 568, L35

Narayan, R., & Yi, I. 1995, ApJ, 452, 7101

Nishimura, J., Mitsuda, K., & Itoh, M. 1986, PASJ, 38, 819

Oosterbroek, T., Barret, D., Guainazzi, M., & Ford, E. C. 2001, A&A, 366, 138

Parmar, A., Martin, D. D. E, Bavdaz, M., et al. 1997, A&AS, 122, 309

Piraino, S., Santangelo, A., Kaaret., P., et al. 1999, A&A, 349, L77

Schultz, J. 2002 [`astro-ph/0210250`]

Shimura, T., & Takahara, F. 1995, ApJ, 445, 780

Singh, K. P., Apparao, K. M. V. & Kraft, R. P. 1994, ApJ, 753, 761 (S94)

Smale, A. P. 1991, PASP, 103, 636

Smith, H. A., Beall, J. H., & Swain, M. R. 1990, AJ, 99, 273

Sztajno, M., van Paradijs, J., Lewin, W. H. G., et al. 1986, MNRAS, 222, 499

Sunyaev, R. A., & Titarchuk, L. 1980, A&A, 86, 121

Swank, J .H., Becker, R. H., Boldt, E. A., et al. 1978, MNRAS, 182, 349

Titarchuk, L. G. 1994, ApJ, 434, 570

van der Klis, M., Hasinger, G., Damen, E., et al. 1990, ApJ, 360, L19

van der Klis, M. 1995, in X–ray Binaries, ed. W. H. G. Lewin, J. van Paradijs, & E. P. J. van den Heuvel (Cambridge Univ. Press), 252

van Paradijs, J., & McClintock, J. E. 1995, in X–ray Binaries, ed. W. H. G. Lewin, J. van Paradijs, & E. P. J. van den Heuvel (Cambridge Univ. Press), 536

Wallace, R. K., Woosley, S. E., & Weaver, T. A. 1982, ApJ, 258, 696

Warwick, R. S., Marshall, N., Fraser, G. W., et al. 1981, MNRAS, 197, 865

Wendker, H. J. 1995, A&AS, 109, 177

White, N. E., Peacock, A., Hasinger, G., et al. 1986, MNRAS, 218, 129

White, N. E., Stella, L., & Parmar, A. N. 1988, ApJ, 324, 363

White, N. E., Kallman, T. R., & Angelini, L. 1997, in X–ray imaging and Spectroscopy of Cosmic Hot Plasmas, ed. F. Makino, & K. Mitsuda (Tokio: Universal Academy Press), 411